Novel protein ADTRP regulates TFPI expression and function in human endothelial cells in normal conditions and in response to androgen

Cristina Lupu,[1] Hua Zhu,[1] Narcis I. Popescu,[1,2] Jonathan D. Wren,[3] and Florea Lupu[1,2]

[1]Cardiovascular Biology Research Program, Oklahoma Medical Research Foundation, Oklahoma City, OK; [2]Department of Pathology, University of Oklahoma Health Sciences Center, Oklahoma City, OK; and [3]Arthritis and Clinical Immunology Research Program, Oklahoma Medical Research Foundation, Oklahoma City, OK

Thrombosis and cardiovascular disease (CVD) represent major causes of morbidity and mortality. Low androgen correlates with higher incidence of CVD/thrombosis. Tissue Factor Pathway Inhibitor (TFPI) is the major inhibitor of tissue factor-factor VIIa (TF-FVIIa)–dependent FXa generation. Because endothelial cell (EC) dysfunction leading to vascular disease correlates with low EC-associated TFPI, we sought to identify mechanisms that regulate the natural expression of TFPI. Data mining of NCBI's GEO microarrays revealed strong coexpression between TFPI and the uncharacterized protein encoded by *C6ORF105*, which is predicted to be multispan, palmitoylated and androgen-responsive. We demonstrate that this protein regulates both the native and androgen-enhanced TFPI expression and activity in cultured ECs, and we named it androgen-dependent TFPI-regulating protein (ADTRP). We confirm ADTRP expression and colocalization with TFPI and caveolin-1 in ECs. ADTRP-shRNA reduces, while over-expression of ADTRP enhances, TFPI mRNA and activity and the colocalization of TF-FVIIa–FXa-TFPI with caveolin-1. Imaging and Triton X-114–extraction confirm TFPI and ADTRP association with lipid rafts/caveolae. Dihydrotestosterone up-regulates TFPI and ADTRP expression, and increases FXa inhibition by TFPI in an ADTRP- and caveolin-1-dependent manner. We conclude that the ADTRP-dependent up-regulation of TFPI expression and activity by androgen represents a novel mechanism of increasing the anticoagulant protection of the endothelium. (*Blood*. 2011;118(16):4463-4471)

Introduction

Cardiovascular disease (CVD) is a major cause of morbidity and mortality, with men having higher rates of clinical events than women.[1] Testosterone serves many physiologic functions,[2] including cardio-protective effects, and its decline with advancing age parallels impaired physical, sexual and cognitive functions. It is believed that androgen replacement therapy could benefit the declining functions in the elderly, as well as reverse the adverse effects of androgen deficiency on men's health in diabetes, metabolic syndrome and CVD.[3,4]

Tissue factor pathway inhibitor (TFPI) is a key natural inhibitor of coagulation: it neutralizes factor Xa (FXa) and inhibits tissue factor-factor VIIa (TF-FVIIa) in the presence of FXa. In vivo most of TFPI is on endothelial cells (ECs), reversibly bound to yet unidentified receptors, and glycosyl phosphatidylinositol-anchored to caveolae/lipid rafts.[5-8] The cell-associated form of TFPI, as opposed to the soluble, variably truncated forms of the inhibitor, is considered the most physiologically significant inhibitor of TF-FVIIa.[7,9] Frequent thrombotic events associate with comorbidities (cancer, diabetes, and CVD) in older people. TF-driven coagulation not adequately countered by TFPI seemingly underlies thrombotic complications in sepsis, atherosclerosis, lupus and cancer,[10-14] and could associate with increased risk of deep vein thrombosis/venous thromboembolism (DVT/VTE).[15-18] Although TFPI is a major endogenous inhibitor of coagulation, few mechanisms/factors that regulate the natural expression of TFPI have been identified so far.[19-22] Finding ways to up-regulate the cell-associated TFPI to prevent unwanted clotting and to inhibit TF-dependent pathologic effects, although being of great importance, is a still under-investigated area. Here we applied the previously described global meta-analysis (GAMMA) of NCBI's Gene Expression Omnibus (GEO) 2-channel human microarray datasets[23] to reveal genes that *TFPI* was coexpressed with. The approach identified *C6ORF105*, a potentially androgen-inducible gene (AIG), as a very high scoring gene coexpressed with both *TFPI* and several other genes associated with TFPI in the literature.

ECs are a key regulator of cardiovascular function. Unregulated production of enzymes/inhibitors that control coagulation and fibrinolysis, and of vasodilating agents, is a major consequence of endothelial dysfunction. Beneficial effects of androgens include enhanced production of antithrombin III, tissue-type plasminogen activator and nitric oxide, and reduced plasminogen activator inhibitor-1.[24] The limited available data concerning the effects of androgens on TFPI in vitro[25-27] and in patients[28,29] also point toward a positive correlation.

The present study analyzes the contribution of this novel protein to the anticoagulant function of TFPI in ECs in culture, and its regulation by androgens. We report for the first time that the protein encoded by *C6ORF105*, acting as a novel androgen-controlled membrane protein, regulates TFPI expression and function in ECs. We tentatively named it androgen-dependent TFPI regulating protein (ADTRP). We hypothesize that this novel aspect of the TFPI-dependent anticoagulant mechanism may increase the

Submitted May 19, 2011; accepted August 14, 2011. Prepublished online as *Blood* First Edition paper, August 25, 2011; DOI 10.1182/blood-2011-05-355370.

The online version of this article contains a data supplement.

The publication costs of this article were defrayed in part by page charge payment. Therefore, and solely to indicate this fact, this article is hereby marked "advertisement" in accordance with 18 USC section 1734.

protection of the endothelium in pathologic conditions like CVD, DVT/VTE, sepsis, and cancer.

Methods

Tools for investigation of ADTRP expression

C-terminus double-tagged (Myc and DDK/FLAG) *pCMV6-Entry/C6ORF105* expression vector, C6orf105 recombinant protein (here after named ADTRP) overexpressed in HEK293 (positive control), HuSH 29-mer shRNA expression *pRS* vectors and controls (noneffective 29-mer scrambled shRNA cassette in *pRS*), and mAbs anti FLAG/DDK, were all from OriGene. Rabbit polyclonal antibodies were custom produced and purified at EZBiolab Inc, using as antigen 2 peptides of the ADTRP predicted extracellular domains: C-V_{143}LRPHSYPSKKYGLT$_{157}$-NH_2 and C-E_{212}EKLNHWKWGDMRQ$_{224}$-NH_2.

Reagents, cells, and tissues

Primary and fluorophore- or peroxidase-conjugated secondary antibodies, human coagulation factors, and cell culture media and supplements were essentially as described.[5,6,30,31] Unconjugated and fluorophore-conjugated monovalent Fab fragments of affinity-purified secondary antibodies for double labeling of primary antibodies from the same host species were from Jackson ImmunoResearch and used according to the manufacturer's protocols. The immortalized hybrid EC line EA.hy926[32] (gift from Dr Cora-Jean Edgell, University of North Carolina) and primary human umbilical vein ECs (HUVECs), which share common morphologic and functional characteristics,[33,34] were used as described.[5,6,30,31] The model systems included: native ECs; cells permanently expressing low levels of TF-YFP,[31] hereafter named TF-EC; ECs and TF-ECs with transiently silenced ADTRP using HuSH 29-mer shRNA expression *pRS* vectors; EC and TF-EC lines stable expressing Cav-1–shRNA, achieved through HuSH system; and, EC and TF-EC expressing the Myc/DDK (FLAG)–tagged protein encoded by *C6ORF105* (here after named ADTRP-FLAG). Cells were transfected with Effectene (QIAGEN).[6] Stable cell lines were selected with 0.5 μg/mL G418. Selected HUVEC lines were used for up to 5 passages. All assays were run on native, mock- and control-transfected cells. Normal baboon lung and aorta, and human placenta samples were collected during previous experiments,[10,35] all approved by IACUC and IRB committees of the Oklahoma Medical Research Foundation and the University of Oklahoma Health Sciences Center.

EC treatments

ECs pre-incubated for 48 hours in medium with 10% steroid-free FBS (charcoal/dextran-stripped; Gemini Bioproducts) were incubated for 24 hours with 30nM (physiologic concentration) of 5-α-androstan-17ß-ol-3-1 (dihydrotestosterone [DHT]; Sigma-Aldrich).

TFPI activity assay

The inhibitory capability of cell surface TFPI was measured by 2-stage functional chromogenic assays on TF-EC monolayers, where TF-FVIIa–dependent FXa generation was quantified in the presence and absence of inhibitory anti-TFPI antibodies, as described.[6,10,11,31]

Immunofluorescence and image analysis

Immunofluorescence and image analysis were used to study the distribution of TFPI, TF, ADTRP, Cav-1, and the raft-specific ganglioside GM_1[5,6,36,37]. By performing the immunostaining at the end of the functional assays, on EC fixed with 3% paraformaldehyde ± permeabilization with 0.1% Triton X-100, we defined the colocalization of the inhibitory TF-FVIIa–FXa-TFPI quaternary complex with rafts/caveolae as an index of the down-regulation of the coagulation pathway.[6] Controls included pre-immune sera (for the rabbit anti-ADTRP IgG), irrelevant or isotype-matched IgGs, and omission of primary antibodies. Images were collected with a Nikon C1 confocal system on a Nikon TE2000U microscope (Nikon Instruments Inc) using computer-controlled lasers and a PlanApochromat oil-immersion objective (×60, NA: 1.4). The acquisition software was EZ-C1 Version 3.6 (Nikon Corporation). Image collection parameters (neutral density filters, pinhole, and detector gains) were kept constant during image acquisition to make reliable comparisons between specimens.[10,11,35] Image acquisition was done sequentially for each fluorescence channel to avoid bleed through. Mean fluorescence intensity (MFI), expressed in arbitrary units (AU) was measured on a minimum of 50 cells per group randomly chosen from at least 5 different pictures for each experimental condition. The colocalization quantification, performed by Adobe Photoshop (Adobe Systems), comprised series of subtraction of the fluorescence intensity of individual and overlapping and nonoverlapping channels, and expression of the overlap as mean percentage of the total signal for each channel, essentially as described.[6]

Quantitative real-time (qRT) PCR

qRT-PCR was used to measure TFPI, ADTRP, and Cav-1 mRNA.[35] Total RNA was isolated with the RNeasy Mini kit, with extra DNase digestion of RNA using RNase-free DNase Set (both kits were from QIAGEN). Primers were designed using Primer Express software (Applied Biosystems). qRT-PCR was conducted on an ABI Prism 7000 Sequence Detection System (Applied Biosystems). iTaqTM SYBR Green Supermix (Bio-Rad) was used for detection and quantitation according to the manufacturer's protocol. Data are expressed either as C_t values (cycle threshold; the cycle at which the fluorescence signal was statistically significant over background), or as the ratio of the target gene in the experimental groups relative to the control samples, corrected for the reference gene (18S rRNA). For the latter approach we used the $\Delta\Delta C_T$ method (http://www.appliedbiosystems.com/).

Other assays

Cell and tissue lysis, Western blot, and Triton X-114 cellular fractionation, were performed as described,[6] except for using chemiluminescent detection (GE Healthcare). Densitometric analysis used ImageJ 1.42b software (National Institutes of Health). Total protein was assayed by BCA (Pierce). A modified ELISA performed directly on fixed EC monolayers[5] using a FLUOstar Omega multimode microplate reader (BMG LABTECH), measured TFPI and ADTRP levels associated with the cells, separately on the cell surface and on cells permeabilized with 0.01% saponin. We expressed the antigen levels as ratios between the absorbance of the peroxidatic reaction (measured at 450-nm after cleavage of *ortho*-phenylenediamine [OPD; Sigma] substrate) and the fluorescence intensity of DAPI, the latter added to the EC monolayers for cell number normalization. Flow cytometry was performed on fixed cells as described,[31] using a FACScan flow cytometer and CellQuest Pro Version 5.2 (BD Bioscience).

Data collection and statistical analysis

All results are reported as mean ± SD for activity assays and mean ± SEM for qRT-PCR and image analysis. We used Prism Version 5.0c (GraphPad) to perform the unpaired *t* test, 1-way ANOVA, and Pearson's correlation analysis. Differences were considered significant when $P < .05$. All experiments were repeated at least 3 times unless otherwise mentioned. n indicates number of experiments, with each assay typically run in triplicate.

Results

Androgen-dependent TFPI regulating protein (ADTRP): a novel protein that coregulates with TFPI

We used the previously reported[23] and validated[38] in silico data mining approach to identify novel genes associated with *TFPI*. The method used a global meta-analysis (GAMMA) of NCBI's GEO 2-color microarray datasets to identify genes that were consistently and specifically coexpressed with each other across heterogeneous conditions, and was guided by a literature-based analysis of the

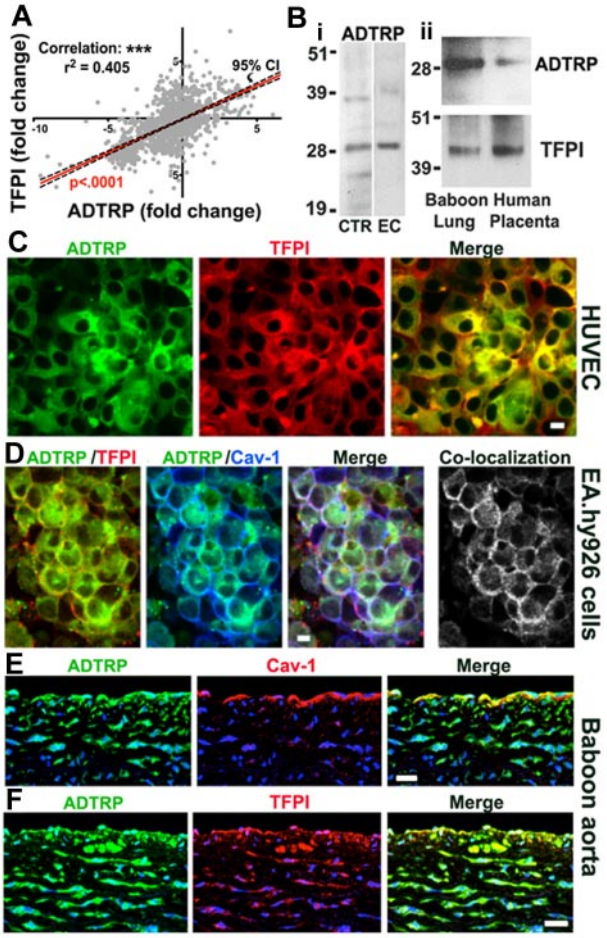

Figure 1. Analysis of the expression and cellular distribution of ADTRP, a novel protein that coregulates with TFPI. (A) Coexpression plot (red) of *ADTRP* and *TFPI* resulted from the GAMMA of GEO microarrays shows significant positive correlation between the expression levels (represented as fold-change) of the 2 genes. $P < .0001$ for the slope's deviation from zero. n = 1500. Confidence interval (CI; 95%) is shown as black interrupted lines. (B) Western blot performed on (i) cellular lysates of HEK293T (positive control, lane CTR) and EAhy926 (lane EC), and (ii) tissue extracts of normal baboon lung and human placenta, using rabbit anti-ADTRP and anti-TFPI IgGs for probing. (C-F) Immunofluorescence and confocal microscopy show the localization of ADTRP in human ECs in culture and the baboon aorta. Non-permeabilized HUVECs (C) were immunostained for cell surface ADTRP (FITC, green) and TFPI (Cy_3, red). EA.hy926 cells (D) were first immunostained for cell surface ADTRP (FITC, green) and TFPI (Cy_3, red), then permeabilized and immunolabeled for Cav-1 (Cy_5, blue). Overlap (white) designates the colocalization channels obtained by Adobe Photoshop image analysis. Baboon aorta sections were immunostained for ADTRP (FITC, green) and Cav-1 (E) or TFPI (F; Cy_3, red for both) after brief permeabilization.[10,11] Blue: nuclear staining. Bars: (C-D) 10 μm; (E-F) 50 μm.

published associations of the coregulated genes (details in supplemental Methods and Tables 1-3, available on the *Blood* Web site; see the Supplemental Materials link at the top of the online article). Based on the relative frequencies of each term in MEDLINE, the association was significant ($P < .01$). *C6ORF105* (Entrez Gene ID 84 830; chromosome location 6p24.1) was chosen for analysis from among the highest-scoring unknown genes. As shown in Figure 1A, *C6ORF105 (ADTRP)* has a strong pattern of parallel coexpression with *TFPI*, and a statistically significant positive correlation (Pearson's r: 0.636; r^2: 0.405; slope deviation from zero highly significant).

According to UniProtKB/Swiss-Prot, the protein encoded by *C6ORF105* (Protein Q96IZ2) is likely to have 2 isoforms, M_w ~ 27-29 kDa, and 3-6 predicted trans-membrane domains. Details about sequences and putative domains are given in supplemental Figure 1. Based on sequence similarities, this protein belongs to the AIG family. AIG1 was cloned from human dermal papilla cells and is homologous to hamster FAR-17a.[39] The in vivo function of the protein encoded by *C6ORF105* is yet unknown.

ADTRP is expressed in cultured ECs and various tissues

qRT-PCR verified that ADTRP was expressed in both HUVECs and EAhy926, as well as in the baboon lung. C_t values (mean ± SEM) for ADTRP mRNA expression were, 22.5 ± 0.7 for HUVECs (n = 8) and 23.10 ± 0.61 for EA.hy926 cells (n = 12), which are strong positive reactions indicative of abundant mRNA. For the baboon lung, C_t = 34.5 ± 0.91 (n = 4).

Western blot using our custom-made anti-ADTRP IgG revealed bands consistent with the predicted M_r (~ 28 kDa) of the *C6ORF105*-encoded protein in the positive control from OriGene (Figures 1Bi lane CTR; FLAG-tagged protein encoded by *C6ORF105* expressed in HEK293T cells). The fusion protein is hereafter designated ADTRP-FLAG. Endogenously expressed ADTRP was similarly detected in lysates of EA.hy926 cells (Figure 1Bi lane EC), HUVECs (see Figure 2A lane 1), and baboon lung and human placenta (Figure 1Bii). For the latter, probing with anti-TFPI IgG is also shown for comparison.

By immunofluorescence, ADTRP colocalized with TFPI on the cell surface (Figure 1C, HUVEC), and with both TFPI and Cav-1 intracellularly (not shown). The percentage of TFPI colocalizing with ADTRP (and reciprocal) was ~ 65% for the cell surface and ~ 80% in permeabilized cells. After applying our previously described triple immunostaining approach[6] to detect TFPI and ADTRP on the cell surface and Cav-1 after permeabilization (Figure 1D), we calculated a mean overlap of 75% between cell surface TFPI and ADTRP and sub-membrane Cav-1, with ~ 65% of ADTRP itself overlapping Cav-1. Control immunostaining using the rabbit pre-immune sera, as well as irrelevant rabbit IgG and omission of the first antibody, all gave negative results (not shown).

In the baboon aorta, ADTRP colocalized with Cav-1 in the endothelium and with TFPI in both the endothelium and smooth muscle cells (Figure 1E-F).

Posttranscriptional silencing of ADTRP in ECs in vitro

ADTRP mRNA measured by qRT-PCR in HUVECs at 72 hours after transfection with ADTRP-shRNA–expression vectors decreased by ~ 3-fold. Concomitantly, TFPI mRNA was also 1.75 times lower (see also Figure 7A white bars-Control).

Western blot densitometry revealed that HUVEC transiently expressing ADTRP-shRNA displayed > 2-fold reduction in ADTRP levels after normalization to ß-actin, compared with controls (Figure 2A; lane 1: nontargeting shRNA; lane 2: ADTRP-shRNA). TFPI also decreased ~ 1.3-fold (Figure 2A). Transfection efficiency, verified with an EGFP-expressing vector,[6] was ~ 80%.

The cell surface expression of ADTRP decreased 2.8-fold, and that of TFPI by 1.7 times (Figure 2B-C; semiquantitative analysis after immunostaining). Cav-1 levels were not significantly affected, either as mRNA (~ 1.15-fold increase by qRT-PCR) or as protein (Figure 2B-C).

Correlation analysis of TFPI and ADTRP fluorescence intensity on the cell surface of 20 individual cells (Figure 2D) revealed highly significant positive correlation between the levels of the 2 proteins for both controls (r^2: 0.927) and ADTRP-shRNA ECs (r^2: 0.896).

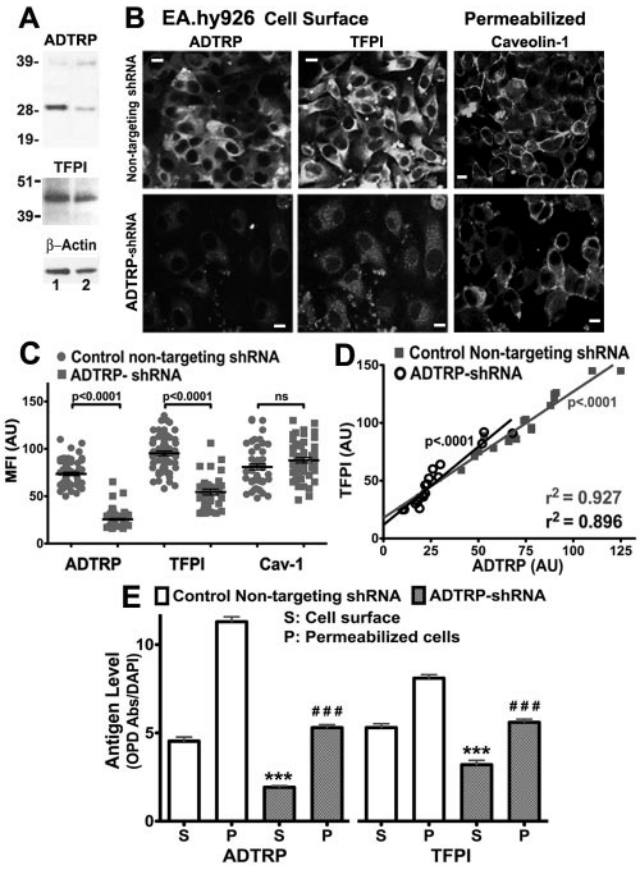

Figure 2. ADTRP post-transcriptional silencing decreases ADTRP and TFPI expression. (A) Total lysates of HUVECs transiently expressing nontargeting shRNA (control, lane 1) or ADTRP-shRNA (lane 2) were analyzed by SDS-PAGE and immunoblotting with rabbit anti-ADTRP, anti-TFPI IgGs, and mAb anti ß-actin. (B) Immunostaining for cell surface ADTRP and TFPI, and Cav-1 after permeabilization, on EA.hy926 cells transiently expressing nontargeting shRNA or ADTRP-shRNA. Bars: 10 μm. (C) Scatter-plot and statistical analysis (1-way ANOVA) of MFI for ADTRP, TFPI and Cav-1 in control EC (nontargeting shRNA) and EC expressing ADTRP-shRNA. MFI was measured on > 50 individual cells per experimental condition and expressed as arbitrary units (AU). Data are mean ± SEM. (D) Correlation analysis performed on individual cells, either control or ADTRP-shRNA EC, to analyze the relationship between ADTRP and TFPI fluorescence levels on the EC surface. r^2 and slope deviation from 0 are highly significant for both experimental conditions. (E) ELISA on control ECs and ADTRP-shRNA cell monolayers (24-well plates) shows antigen levels for ADTRP and TFPI on the cell surface (S) and in permeabilized cells (P). Antigen values are expressed as ratios between the absorbance measured at 450 nm after developing the peroxidatic reaction with OPD, and the fluorescence intensity of DAPI used for normalization of cell numbers. Data are mean ± SEM; n = 6. ***,###: $P < .001$ versus control cells (unpaired *t* test).

The ELISA performed on cell monolayers confirmed significant reduction of ADTRP and TFPI after ADTRP silencing, both on the cell surface and in permeabilized cells (Figure 2E).

ADTRP silencing in TF-EC reduced the TF/TFPI colocalization to ~ 44% of the total TF, down from ~ 63% measured in the control TF-EC (Figure 3A-B). The percentage of TF overlapping both TFPI and Cav-1 decreased even more, by > 2-fold, compared with control TF-EC, thus leaving the majority of TF (~ 80%) outside the colocalization with TFPI and Cav-1 (Figure 3A-B; triple overlap white, and nonoverlapping TF green).

The inhibitory capability of cell surface TFPI against TF-FVIIa-triggered FXa generation was measured in TF-EC cells, as described.[6,31,40] The difference between total FXa generated in the presence of inhibitory anti-TFPI IgG and the FXa generated in the absence of the antibody represents the amount of FX(a) whose activation was prevented by, or which was inhibited by TFPI, therefore giving the measure of the functional potency of cell surface TFPI. TFPI-dependent FXa inhibition was ~ 3-times reduced in ADTRP-shRNA EC (Figure 3C red bars). Whereas TFPI in control ECs inhibited ~ 55% of the total FXa generated, the inhibitory capability of TFPI in ADTRP-shRNA cells was only ~ 12%. All values were normalized to 10^6 cells.

Overexpression of ADTRP in ECs

By qRT-PCR, the mRNA expression of ADTRP and TFPI increased 3-fold and 1.6-fold, respectively, in both EA.hy926 and HUVECs stable expressing ADTRP-FLAG (see also Figure 7A white bars-Control).

Using Western blot we first verified the specificity of the anti-FLAG mAb. Figure 4Ai, shows the band of ~ 28 kDa labeled by anti-FLAG in the positive control (lane 1), but not in the negative one (lane 2). Densitometry of western blots probed with the rabbit anti-ADTRP IgG (Figure 4Aii) revealed that EA.hy926 cells stable expressing ADTRP-FLAG (lane 2) displayed ~ 3-fold enhanced ADTRP compared with control cells (lane 1; values normalized to ß-actin). Anti-FLAG mAb stained the same band in the transfected cells, but gave no signal in control EC (Figure 4Aii). TFPI also increased by ~ 1.5-fold versus control EC (not shown).

HUVEC lines stable expressing ADTRP-FLAG displayed robust immunostaining with anti-FLAG, and strong colocalization with both ADTRP (> 93%) and TFPI (80%) on the cell surface (Figure 4B overlap appears white). The cell surface expression of both proteins increased significantly versus control EC, by > 2-fold for ADTRP and 1.5-fold for TFPI (Figure 4C). The triple

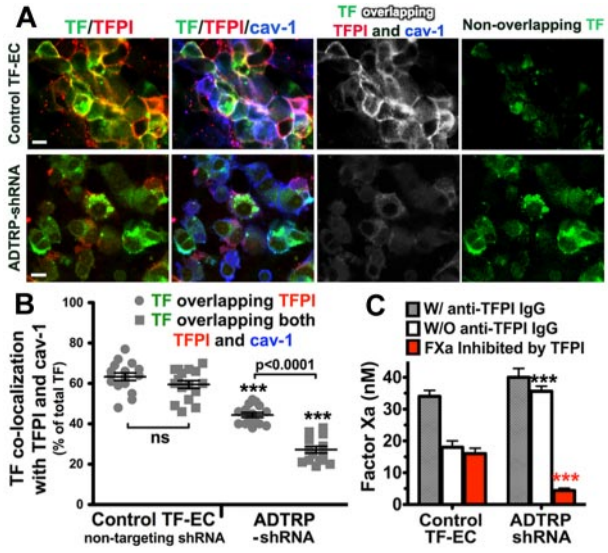

Figure 3. Silencing of ADTRP decreases cell surface TFPI expression and activity. (A) Immunofluorescence and confocal microscopy showing the distribution and colocalization of cell surface TFPI (Cy_3, red) with YFP-TF (YFP, green) and Cav-1 (Cy_5, blue; after permeabilization) on controls (nontargeting shRNA) and ADTRP shRNA-expressing TF-EC. Triple overlapping (white) and nonoverlapping TF (green) channels were generated by the Adobe Photoshop image analysis. Bars: 10 μm. (B) Scatter-plot and statistical analysis (1-way ANOVA) of the colocalization percentage between TF and TFPI, and TF/TFPI/Cav-1, out of the total MFI of TF. ***$P < .001$ for both sets of data in the ADTRP-shRNA group compared with control (nontargeting shRNA) TF-EC group. ns, $P > .05$ for the difference between the sets of data within the control experimental group. Data are mean ± SEM. (C) The inhibitory capability of cell surface TFPI against TF-FVIIa–dependent FXa generation measured in TF-EC in the presence/absence of inhibitory anti-TFPI IgG. Values are normalized to 10^6 cells. ***$P < .001$ versus control (unpaired *t* test). Data are mean ± SD of triplicates.

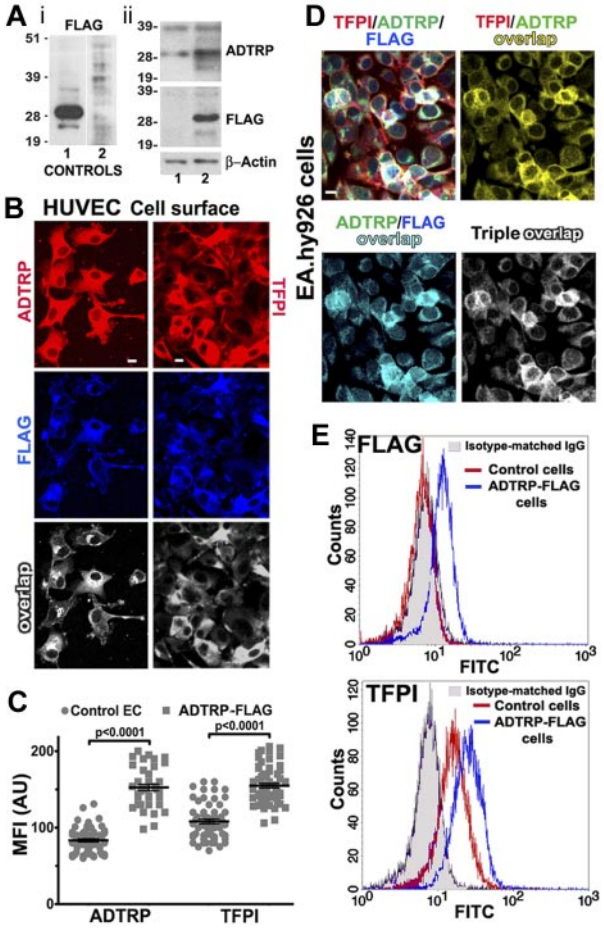

Figure 4. Stable expression of FLAG-tagged ADTRP in ECs. (A) Subpanel i: validation of the anti-FLAG mAb by Western blot of HEK293T lysates, expressing or not ADTRP-FLAG. Lane 1: positive control; lane 2: negative control (both purchased from OriGene). Subpanel ii: Total lysates of EAhy926 cells were analyzed by SDS-PAGE and immunoblotting with rabbit anti-ADTRP IgG and mAbs anti-FLAG and anti–ß-actin. Lane 1: mock-transfected ECs; lane 2: EC line stable expressing ADTRP-FLAG. (B) Cell surface immunostaining with either anti-ADTRP or anti-TFPI (Cy_3, red for both) and anti-FLAG (Cy_5, blue) IgGs on HUVEC line stable expressing ADTRP-FLAG. Overlap (white) designates the colocalization channels resulting from the image analysis. (C) Scatter-plot and statistics (1-way ANOVA) of MFI after immunostaining for cell surface ADTRP and TFPI on control (mock-transfected) and ADTRP-FLAG–expressing HUVECs. Data are mean ± SEM. (D) Immunofluorescence on nonpermeabilized EAhy926 cell line stable expressing ADTRP-FLAG shows the cell surface distribution of TFPI (Cy_3, red), ADTRP (FITC, green) and FLAG (Cy_5, blue) and their double and triple colocalization channels. Bars: 10 μm. (E) Flow cytometric analysis of FLAG and TFPI on the cell surface of control cells and ADTRP-FLAG ECs. The fluorescent profile of mAb anti-FLAG is indistinguishable from the isotype-matched IgG (shaded area) on control cells (red), but shifts on ADTRP-FLAG ECs (blue, top panel). The bottom panel shows the shift in anti-TFPI staining in ADTRP-FLAG ECs (blue) compared with control cells (red).

colocalization TFPI/ADTRP/FLAG on the EC surface showed 85% ADTRP/TFPI overlap, and > 90% of ADTRP and FLAG staining together colocalized with TFPI (Figure 4D). Control immunostaining with mouse isotype-matched IgG, or with anti-FLAG mAb on native ECs, showed negative results (not shown).

Flow cytometry confirmed that the anti-FLAG mAb significantly labeled the cell surface of ECs stable expressing ADTRP-FLAG while not binding to native ECs (Figure 4E FLAG panel). Cell surface TFPI increased by ~ 1.7 times on ADTRP-FLAG ECs versus control cells (Figure 4E TFPI panel).

Over-expression of ADTRP increased the TF/TFPI overlap to ~ 90% up from 63% in control ECs, and enhanced the triple colocalization TF/TFPI/Cav-1 to > 85% of the total TF (Figure 5A-B). TFPI activity increased by 1.6 times in cells expressing ADTRP-FLAG versus control TF-EC (Figure 5C), thus inhibiting ~ 75% of the total FXa generated.

ADTRP shares the same location with TFPI in caveolae/lipid rafts

Cell surface TFPI and FLAG in HUVECs expressing ADTRP-FLAG significantly colocalized with submembrane Cav-1, visualized after cells permeabilization; 85% of FLAG staining overlapped Cav-1, the colocalization of TFPI with Cav-1 increased to > 85% of TFPI (vs 60% in control cells), and > 90% of TFPI and FLAG overlapped Cav-1 (Figure 6A).

Extraction of ECs with Triton X-114 followed by temperature-induced phase separation led to isolation of cell fractions rich in hydrophobic proteins (detergent fraction, D) and fractions containing mainly soluble proteins (water fraction, W). As previously shown for TFPI,[6] ADTRP also predominantly associated with D fractions in both control and ADTRP-FLAG cells (Figure 6B lanes 1 and 3: W fractions; lanes 2 and 4: D fractions; lanes 1 and 2: control ECs; lanes 3 and 4: ADTRP-FLAG). By densitometry, the fold-enrichment of ADTRP in D-fractions versus W-fractions was 3× in both control ECs and ADTRP-FLAG cells. The ratios for TFPI were 2.5× in controls (lanes 1 and 2), and > 4× in cells expressing ADTRP-FLAG (lanes 3 and 4). The D-fraction enrichment of both proteins in ADTRP-FLAG cells versus control ECs was higher than for the equivalent W-fractions: ~ 2-fold for TFPI and 2.5× for ADTRP (lanes 4 vs 2), compared with 1.1× for TFPI and 2× for ADTRP (lanes 3 vs 1). The total increase measured in ADTRP-FLAG cells over control ECs was 2.5-fold for ADTRP and 1.5-fold for TFPI, which mirrors the values observed for whole lysates (see also Figure 4A-B).

ECs incubated live for 30 minutes with FITC-labeled cholera toxin B (CTx-FITC) as a ligand for the lipid raft marker GM_1, showed clustering of TFPI and ADTRP (the latter detected with anti-FLAG mAb) on the cell surface, resulting in 80% colocalization of FLAG with CTx and > 86% of TFPI and FLAG together

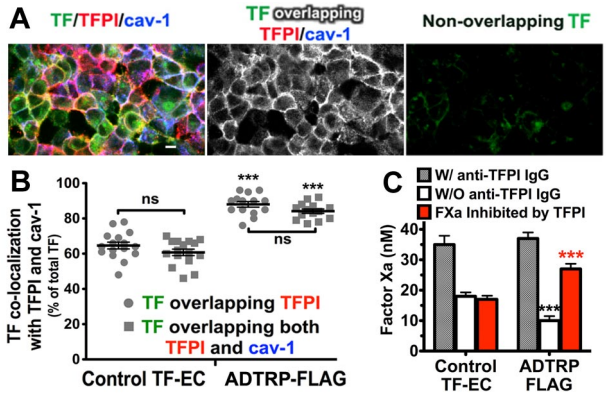

Figure 5. Overexpression of ADTRP increases TFPI expression and activity. (A) Immunofluorescence and confocal microscopy showing the distribution and colocalization of cell surface TFPI (Cy_3, red) with YFP-TF (YFP, green) and Cav-1 (Cy_5, blue; after permeabilization) on TF-EC stable expressing ADTRP-FLAG. Triple overlap (white) and nonoverlapping TF (green) channels result from the image analysis. See also Figure 3A (top panel) for control TF-EC images. Bars: 10 μm. (B) Scatter-plot and statistics (1-way ANOVA) of the colocalization between TF and TFPI, and TF/TFPI/Cav-1, out of the total MFI of TF. Data are mean ± SEM. ***$P < .001$ for both sets of data in the ADTRP-group compared with Control TF-EC group. ns, $P \geq .05$ for the differences between sets of data within the 2 experimental groups. (C) The inhibitory capability of cell surface TFPI against TF-FVIIa–dependent FXa generation measured in TF-EC in the presence/absence of inhibitory anti-TFPI IgG. Values are normalized to 10^6 cells. ***$P < .001$ versus control (unpaired *t* test). Data are mean ± SD of triplicates.

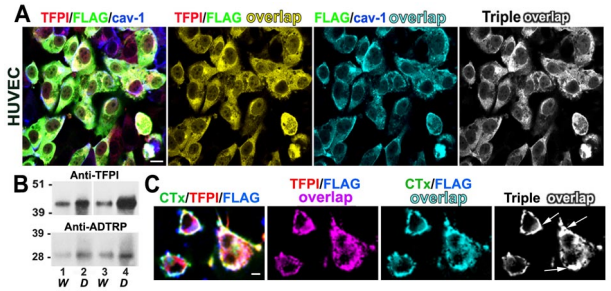

Figure 6. Localization of ADTRP and TFPI in caveolae/lipid rafts. (A) Immunofluorescence shows the distribution and colocalization of cell surface TFPI (Cy_3, red) and FLAG (FITC, green) with Cav-1 (Cy_5, blue; after permeabilization) on HUVEC stable expressing ADTRP-FLAG. Double and triple colocalization channels resulted from image analysis. (B) Representative Western blot with rabbit anti-ADTRP and anti-TFPI IgGs shows the partition of TFPI and ADTRP in the water (W, lanes 1 and 3) and detergent (D, lanes 2 and 4) cellular fractions after extraction with Triton X-114 and phase separation of control ECs (lanes 1 and 2) and stable ADTRP-expressing cells (lanes 3 and 4). (C) Immunofluorescence showing clustering and enhanced colocalization (triple overlap, white) of cell surface TFPI (Cy_3, red) and FLAG (Cy_5, blue) together with Cholera Toxin B (CTx)–FITC (green) after live incubation at 37°C of ADTRP-FLAG-expressing EC with CTx-FITC (ligand for the lipid raft marker GM_1). Bars: 10 μm.

overlapping CTx (Figure 6C; Triple overlap). The colocalization of TFPI with CTx (> 80%) and of FLAG with TFPI (~ 92%) was significantly higher than the equivalent overlapping calculated when pre-fixed cells were incubated with CTx-FITC (control cells): ~ 63% for TFPI/CTx and 80% for FLAG/TFPI (not shown).

Androgen increases TFPI and ADTRP expression and TFPI activity

qRT-PCR showed that the mRNA expression of TFPI and ADTRP significantly increased in both HUVECs and EA.hy926 after incubation with 30nM DHT for 24 hours, by 3-fold for ADTRP and 2-fold for TFPI (Figure 7A Native).

By semiquantitative analysis after immunostaining we calculated ~ 2 times enhanced expression of both TFPI and ADTRP on the EC surface after DHT incubation (Figure 7B-C). Similar increase of total cellular TFPI was observed by Western blot (not shown). Androgen treatment increased the TFPI/Cav-1 overlap to > 75% of the cell surface TFPI, up from ~ 63% in control cells, as well as the TFPI/ADTRP/Cav-1 overlap to ~ 90%, vs 75% in controls (see also Figure 1D).

TFPI-dependent FXa inhibition increased ~ 2-fold in cells incubated with DHT compared with controls (Figure 7D Control TF-EC; compare with controls in Figures 3C and 5C). TFPI in androgen-incubated ECs inhibited 70% of the total FXa generated. The colocalization of TF with TFPI and Cav-1 in TF-EC also increased to > 75% of TF (Figure 7E), versus ~ 63% in control cells (see Figure 3A-B).

Expression of both ADTRP and Cav-1 regulates TFPI response to androgen

TFPI mRNA failed to increase in response to androgen in ADTRP-shRNA EC (Figure 7A ADTRP-shRNA group). Androgen had a marginal effect in Cav-1–shRNA EC, enhancing by only ~ 1.3-times the mRNA expression of TFPI (Figure 7A Cav-1–shRNA group) and ADTRP (not shown). Over-expression of ADTRP also precluded androgen from enhancing TFPI mRNA as in native cells (Figure 7A ADTRP-FLAG group). Interestingly, Cav-1 mRNA was slightly reduced, by ~ 1.4-fold in these cells (not shown).

Androgen enhanced the cell surface TFPI activity by ~ 2-fold in native TF-EC, but failed to significantly increase TFPI-dependent FXa inhibition in ADTRP-shRNA ECs and in Cav-1–shRNA EC (Figure 7D red bars; compare with Figure 3C). In these cells, TFPI inhibited only ~ 11% of the total FXa generated. Androgen increased by 1.6-times the already high TFPI activity in ADTRP-FLAG cells (Figure 7D; compare with Figure 5C), raising the inhibition of FXa to ~ 95%.

Cav-1 silencing reduced cell surface TFPI by > 3-fold (MFI ± SEM: 38 ± 1.2 AU) compared with control cells (see Figure 2C; nontargeting shRNA ECs, MFI ± SEM: 95 ± 2.4 AU), but had no significant effect on ADTRP (Figure 7F Control; MFI: 71 ± 3.6 AU; versus 73 ± 2 in control cells, see Figure 2B-C).

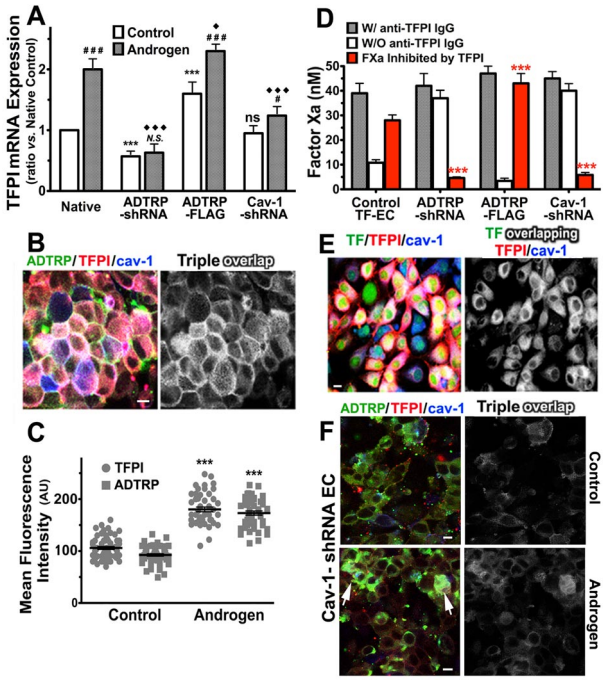

Figure 7. Androgen regulates the expression and distribution of TFPI and ADTRP, and TFPI activity. (A) mRNA expression of TFPI assayed by qRT-PCR in control ECs (open bars) and cells incubated with 30nM DHT for 24 hours (gray bars). The effect of DHT was studied in Native cells, and in ADTRP-shRNA–, ADTRP-FLAG–, and Cav-1-shRNA–expressing EAhy926 cells. Values are presented as fold-change from native control ECs after correction for 18S rRNA as internal control. Experiments were repeated twice and run in triplicate. (B) Immunostaining for ADTRP (FITC, green) and TFPI (Cy_3, red) on the cell surface, and Cav-1 (Cy_5, blue) after permeabilization on HUVECs treated with DHT. Overlap (white) designates the colocalization channel resulting from the image analysis. (C) Scatter-plot and statistics (1-way ANOVA) of MFI of cell surface TFPI and ADTRP measured on cells processed as in panel (B). Control cells were treated similarly to the Androgen-group but without DHT. Data are mean ± SEM. ***$P < .001$ for both sets of data in the Androgen-group compared with the Control-group. (D) Effect of DHT on the inhibitory capability of cell surface TFPI against TF-FVIIa–dependent FXa generation measured in TF-EC in the presence/absence of inhibitory anti-TFPI IgG. Values are normalized to 10^6 cells. Data are mean ± SD of triplicates. The groups of cells and DHT treatment were as described in panel A. (E) Immunofluorescence and confocal microscopy show the effect of DHT on the distribution and colocalization of cell surface TFPI (red) with YFP-TF (green) and Cav-1 (blue; after permeabilization) on TF-EC. Triple overlap (white) channel resulted from the image analysis. (F) Immunofluorescence for cell surface TFPI (Cy_3, red) and ADTRP (FITC, green), and Cav-1 (Cy_5, blue; after permeabilization) in EC stable expressing Cav-1–shRNA, either native (Control) or incubated with DHT (Androgen). Overlap (white) designates the triple colocalization channel. White arrows: residual Cav-1 expression. (A, D) Statistical analysis was performed by 1-way ANOVA. *,#,♦: $P < .05$, **,##,♦♦: $P < .01$, ***,###,♦♦♦: $P < .001$, *N.S.* and ns, $P \geq .05$. Asterisks (*) and ns: difference versus Native within the Control-group. Diamonds (♦): difference versus Native within the Androgen-group. Pound signs (#) and N.S: difference between Androgen-treated versus Control cells within each experimental group. Bars: 10 μm.

While androgen increased the cell surface exposure of both proteins by 1.4-fold, TFPI levels (MFI: 59 ± 1.8 AU) remained 3-times lower than in androgen-incubated native cells (Figure 7C; MFI: 180 ± 4.6). Even though on few cells ADTRP was enhanced by androgen to a similar extent as in native ECs, this occurred in cells that displayed residual Cav-1 expression (Figure 7F Androgen arrows), and the overall colocalization of TFPI and ADTRP with Cav-1 stayed well below 50% (compare with panel B).

Discussion

Our study unveils a novel mechanism of regulation of TFPI expression and function in human ECs in culture. We show for the first time that an uncharacterized protein encoded by *C6ORF105* regulates TFPI mRNA expression, cellular distribution and cell-associated anticoagulant activity of the inhibitor, both in native conditions and in response to androgen. We tentatively named this novel protein ADTRP.

Although EC-associated TFPI is recognized as the major physiologic inhibitor of the TF-FVIIa–triggered coagulation pathway, few factors/mechanisms that significantly regulate the natural expression of TFPI have been identified so far. The significance of our study is 2-fold. First, we identify a novel EC-expressed protein as a major regulator of TFPI expression and function in vitro; and second, we report that physiologic concentration of testosterone's main metabolite, DHT, increases the mRNA, protein expression and anticoagulant capabilities of cell-associated TFPI in human ECs in culture.

Because the in vivo location and function of ADTRP are not yet known, we first analyzed the natural expression of ADTRP, and found it in ECs in culture, as well as in the human placenta and baboon lung and aorta, colocalizing with both TFPI and Cav-1.

Using posttranscriptional silencing, we achieved strong down-regulation of ADTRP mRNA and protein expression in both HUVEC and EA.hy926 cells, and a concomitant reduction of TFPI mRNA expression and of the cell surface TFPI antigen and activity. The decrease of TFPI cell surface antigen (~ 1.7-fold) though, could not account by itself for the highly impaired capability of TFPI to inhibit TF-FVIIa–dependent FX activation. Accordingly, TFPI inhibited only 12% of the total FXa generated in ADTRP-shRNA–expressing TF-EC, versus 55% in control TF-EC, suggesting that ADTRP actively preserves the anticoagulant potential of TFPI on the ECs surface. We have previously shown that a high percentage of TF and TFPI on the cell surface colocalize with the sub-membrane Cav-1 during and/or after the formation of the TF-FVIIa–TFPI-FXa quaternary complex.[6] Here we confirm and extend this finding, showing that the colocalization of the quaternary complex with caveolae, measured semiquantitatively through the triple overlap TF/TFPI/Cav-1, offers the morphologic confirmation of the functional assays. Cell surface TFPI activity, expressed as percentage of inhibited FXa of the total FXa generated, positively correlates with the percentage of TF that colocalizes with both cell surface TFPI and sub-membrane Cav-1. Silencing of ADTRP left ~ 80% of TF free, out of the colocalization with TFPI and Cav-1. Because the levels of Cav-1 were not affected by ADTRP down-regulation, the effect is likely because of the low level of ADTRP itself, which in turn affects the cell surface distribution and activity of TFPI.

Conversely, overexpression of the FLAG-tagged ADTRP increased the mRNA and protein expression of both ADTRP and TFPI, although the effect was, as expected, significantly stronger for the former. Cell surface TFPI strongly colocalized with ADTRP, FLAG and sub-membrane Cav-1. In TF-EC expressing ADTRP-FLAG, the strong patching of cell surface TFPI with TF during the formation of the quaternary complex increased the overlap with Cav-1 to > 85% of the total TF, which translated into similarly enhanced TFPI-dependent inhibition of FXa.

Although in vitro silencing of ADTRP did not affect the expression of Cav-1, it did reduce the colocalization of cell surface TFPI with Cav-1. Similar with TFPI, ADTRP also partially resides in caveolae/lipid rafts, as revealed by immunofluorescence microscopy and biochemical assays. ADTRP colocalized with sub-membrane Cav-1, and both ADTRP and TFPI were significantly enriched in the hydrophobic proteins-rich (D) fraction after Triton X-114 extraction. The clustering of TFPI together with ADTRP over the cell surface during live cell incubation with CTx, a specific ligand for the lipid raft marker GM_1, also suggests that ADTRP share similar localization with TFPI in cell membrane lipid rafts. The potential palmitoylation sites Cys_7 and $Cys_{62/79}$, and predicted trans-membrane domains could be responsible for ADTRP location in lipid rafts/caveolae. Because overexpression of ADTRP enhanced the D-fraction–associated TFPI significantly more than the W-fraction–located inhibitor, we suggest that ADTRP may represent another lipid raft organizer that affects TFPI distribution and activity, besides its mRNA expression. Our data show that the ADTRP protein itself regulates TFPI, either directly or through transcriptional trans-activation. Because ADTRP is a predicted trans-membrane protein, and by immunostaining it does not relocate to the nuclei after androgen treatment, it is unlikely that it functions as a transcription factor (Tf) by itself. Although it is tempting to speculate that ADTRP may interact with and/or regulate other Tfs, more experiments are needed to address the mechanism of the transcriptional regulation of TFPI expression by ADTRP.

Enhanced expression of TFPI after testosterone treatment in vitro was also reported by another group,[25,26] but, since their data lacked true mechanistic insights, this field of study remained under-investigated. Data mining of GEO array profiles also revealed up-regulation of both ADTRP and TFPI mRNA in a prostate cancer cell line after incubation with DHT for 16 hours (supplemental Figure 2).

Here we report that, as yet unknown effects of androgens, namely the up-regulation of the expression and anticoagulant activity of TFPI in ECs, are mediated, at least in part, through the novel protein ADTRP. Our findings bear considerable physiologic significance, especially since TFPI is notoriously nonresponsive to transcriptional regulation.

The molecular machinery mediating responses to androgens involves both genomic and nongenomic effects. Androgen receptor (AR), widely expressed in vivo,[24] acts as androgen-inducible Tf that binds to androgen-response elements (ARE) to regulate gene expression.[1] Activated AR binds to canonical AREs (AGAACAnnnTGTTCT) or to half-site motifs,[41] and interacts with network(s) of AR-collaborating Tfs.[42]

Several prediction algorithms (http://www.cisred.org; http://gene-regulation.com; and http://www.dcode.org) returned negative results for AREs in TFPI promoter, but found potential half-AREs (AGAACA and TGTTCT) in the ADTRP promoter, similar with the half-AREs identified for FAR-17a,[43] the hamster homolog of the human AIG1. We speculate that the ADTRP-mediated transcriptional regulation of TFPI by androgen may involve potential AREs in the ADTRP promoter and AR-collaborating Tfs, acting through cross-modulation and transactivation.[42]

Nonclassic effects of androgen involve AR interactions with Cav-1 and signaling through caveolae,[44,45] including increasing free $[Ca^{2+}]_i$ levels[46] and activation of kinase-signaling cascades.[42] The association of TFPI with lipid rafts/caveolae, partially controlled by the levels of Cav-1 and caveolae-associated cholesterol, directly impact the formation of the inhibitory quaternary complex and thus the cell surface TFPI activity.[6] Androgen-triggered increase of free $[Ca^{2+}]_i$[46] could enhance the colocalization of TFPI with Cav-1 and lipid rafts, and thus increase TFPI anticoagulant activity.[5,30] Androgen-mediated increase of ADTRP in caveolae may constitute another key factor in the regulation of TFPI distribution and activity. The effect of androgen on TFPI activity needs the presence of Cav-1 and/or intact caveolae, probably because of the need for AR–Cav-1 interactions. Although the modulation of TFPI expression and function by androgen/AR most likely involves transcriptional regulation, the process also requires both ADTRP and Cav-1 proteins, as indicated by our post-transcriptional silencing experiments, through mechanisms that await elucidation.

Our studies advance the knowledge on the effects of androgens and unveil the function of the novel protein ADTRP in enhancing the TFPI-dependent anticoagulant properties of the endothelium. Understanding the effect of androgens on the vascular function is an area of major clinical importance, with potentially enormous healthcare implications as the elderly population is growing fast in the US. We reveal novel mechanism(s) of up-regulation of EC anticoagulant function that could be instrumental for the design of vascular protection strategies whereby cellular TFPI and/or other endothelial intrinsic factors, such as ADTRP, could be manipulated to counteract pro-thrombotic states associated with CVD, DVT/VTE, sepsis, or cancer.

Acknowledgments

The authors thank Dr Cora-Jean Edgell (University of North Carolina, Chapel Hill) for the EAhy926 cells, and Dr Robert Silasi-Mansat in our laboratory for the baboon tissue immunostaining.

This work was supported in part by the American Heart Association (grant 0615595Z, N.I.P), a seed grant from the American Cancer Society (ACS-IRG # IRG-05-066-01, J.D.W), and the National Institutes of Health (R01 GM037704 and R01 GM097747, F.L.; 5P20RR020143, J.D.W).

Authorship

Contribution: C.L. and N.I.P. performed experiments; C.L., J.D.W., N.I.P., and F.L. designed the research, analyzed data, and wrote the paper; J.D.W. performed GAMMA of GEO arrays and analyzed data; and H.Z. performed mRNA expression experiments, analyzed data and contributed to writing the paper.

Conflict-of-interest disclosure: The authors declare no competing financial interests.

Correspondence: Cristina Lupu, Oklahoma Medical Research Foundation, 825 NE 13th St, Oklahoma City, OK 73104; e-mail: cristina-lupu@omrf.org.

References

1. McGrath KC, McRobb LS, Heather AK. Androgen therapy and atherosclerotic cardiovascular disease. *Vasc Health Risk Manag.* 2008;4(1):11-21.
2. Bhasin S, Jasuja R. Selective androgen receptor modulators as function promoting therapies. *Curr Opin Clin Nutr Metab Care.* 2009;12(3):232-240.
3. Traish AM, Saad F, Feeley RJ, Guay A. The dark side of testosterone deficiency: III. Cardiovascular disease. *J Androl.* 2009;30(5):477-494.
4. Manolakou P, Angelopoulou R, Bakoyiannis C, Bastounis E. The effects of endogenous and exogenous androgens on cardiovascular disease risk factors and progression. *Reprod Biol Endocrinol.* 2009;7(1):44.
5. Lupu C, Goodwin CA, Westmuckett AD, et al. Tissue factor pathway inhibitor in endothelial cells colocalizes with glycolipid microdomains/caveolae. Regulatory mechanism(s) of the anticoagulant properties of the endothelium. *Arterioscler Thromb Vasc Biol.* 1997;17(11):2964-2974.
6. Lupu C, Hu X, Lupu F. Caveolin-1 enhances tissue factor pathway inhibitor exposure and function on the cell surface. *J Biol Chem.* 2005; 280(23):22308-22317.
7. Piro O, Broze GJ Jr. Comparison of cell-surface TFPIalpha and beta. *J Thromb Haemost.* 2005; 3(12):2677-2683.
8. Maroney SA, Cunningham AC, Ferrel J, et al. A GPI-anchored co-receptor for tissue factor pathway inhibitor controls its intracellular trafficking and cell surface expression. *J Thromb Haemost.* 2006;4(5):1114-1124.
9. Ahamed J, Belting M, Ruf W. Regulation of tissue factor-induced signaling by endogenous and recombinant tissue factor pathway inhibitor 1. *Blood.* 2005;105(6):2384-2391.
10. Tang H, Ivanciu L, Popescu N, et al. Sepsis-induced coagulation in the baboon lung is associated with decreased tissue factor pathway inhibitor. *Am J Pathol.* 2007;171(3):1066-1077.
11. Lupu C, Westmuckett AD, Peer G, et al. Tissue Factor-Dependent Coagulation Is Preferentially Up-Regulated within Arterial Branching Areas in a Baboon Model of Escherichia coli Sepsis. *Am J Pathol.* 2005;167(4):1161-1172.
12. Westrick RJ, Bodary PF, Xu Z, Shen YC, Broze GJ, Eitzman DT. Deficiency of tissue factor pathway inhibitor promotes atherosclerosis and thrombosis in mice. *Circulation.* 2001;103(25): 3044-3046.
13. Elmann A, Sharabi A, Dayan M, Zinger H, Ophir R, Mozes E. Altered gene expression in mice with lupus treated with edratide, a peptide that ameliorates the disease manifestations. *Arthritis Rheum.* 2007;56(7):2371-2381.
14. Versteeg HH, Schaffner F, Kerver M, et al. Inhibition of tissue factor signaling suppresses tumor growth. *Blood.* 2008;111(1):190-199.
15. Dahm A, Van Hylckama Vlieg A, Bendz B, Rosendaal F, Bertina RM, Sandset PM. Low levels of tissue factor pathway inhibitor (TFPI) increase the risk of venous thrombosis. *Blood.* 2003;101(11):4387-4392.
16. Duering C, Kosch A, Langer C, Thedieck S, Nowak-Gottl U. Total tissue factor pathway inhibitor is an independent risk factor for symptomatic paediatric venous thromboembolism and stroke. *Thromb Haemost.* 2004;92(4):707-712.
17. Bladbjerg EM, Madsen JS, Kristensen SR, et al. Effect of long-term hormone replacement therapy on tissue factor pathway inhibitor and thrombin activatable fibrinolysis inhibitor in healthy postmenopausal women: a randomized controlled study. *J Thromb Haemost.* 2003;1(6):1208-1214.
18. Hoke M, Kyrle PA, Minar E, et al. Tissue factor pathway inhibitor and the risk of recurrent venous thromboembolism. *Thromb Haemost.* 2005;94(4): 787-790.
19. Thyzel E, Kohli S, Siegling S, Prante C, Kleesiek K, Gotting C. Relative quantification of glycosaminoglycan-induced upregulation of TFPI-mRNA expression in vitro. *Thromb Res.* 2007;119(6):785-791.
20. Steffel J, Iseli S, Arnet C, Luscher TF, Tanner FC. Cocaine unbalances endothelial tissue factor and tissue factor pathway inhibitor expression. *J Mol Cell Cardiol.* 2006;40(5):746-749.
21. Shimokawa T, Yamamoto K, Kojima T, Saito H. Down-regulation of murine tissue factor pathway inhibitor mRNA by endotoxin and tumor necrosis factor-alpha in vitro and in vivo. *Thromb Res.* 2000;100(3):211-221.
22. Liu W, Zhu ZQ, Wang W, Zu SY, Zhu GJ. Crucial roles of GATA-2 and SP1 in adrenomedullin-affected expression of tissue factor pathway inhibitor in human umbilical vein endothelial cells exposed to lipopolysaccharide. *Thromb Haemost.* 2007;97(5):839-846.
23. Wren JD. A global meta-analysis of microarray expression data to predict unknown gene functions and estimate the literature-data divide. *Bioinformatics.* 2009;25(13):1694-1701.
24. Goglia L, Tosi V, Sanchez AM, et al. Endothelial regulation of eNOS, PAI-1 and t-PA by testosterone and dihydrotestosterone in vitro and in vivo. *Mol Hum Reprod.* 2010;16(10):761-769.
25. Jin H, Lin J, Fu L, et al. Physiological testosterone stimulates tissue plasminogen activator and tissue factor pathway inhibitor and inhibits plasminogen activator inhibitor type 1 release in endothelial cells. *Biochem Cell Biol.* 2007;85(2): 246-251.
26. Jin H, Wang DY, Mei YF, et al. Mitogen-activated protein kinases pathway is involved in physiological testosterone-induced tissue factor pathway inhibitor expression in endothelial cells. *Blood Coagul Fibrinolysis.* 2010;21(5):420-424.
27. Andreotti F, Ferrante G, Crea F. Testosterone, tissue factor inhibition and vascular aging. *Thromb Haemost.* 2010;103(1):9-10.
28. Agledahl I, Brodin E, Svartberg J, Hansen JB.

Plasma free tissue factor pathway inhibitor (TFPI) levels and TF-induced thrombin generation ex vivo in men with low testosterone levels. *Thromb Haemost.* 2009;101(3):471-477.

29. Agledahl I, Brodin E, Svartberg J, Hansen JB. Impact of long-term testosterone treatment on plasma levels of free TFPI and TF-induced thrombin generation ex vivo in elderly men with low testosterone levels. *Thromb Haemost.* 2009;102(5):945-950.
30. Lupu C, Poulsen E, Roquefeuil S, Westmuckett AD, Kakkar VV, Lupu F. Cellular effects of heparin on the production and release of tissue factor pathway inhibitor in human endothelial cells in culture. *Arterioscler Thromb Vasc Biol.* 1999;19(9):2251-2262.
31. Popescu NI, Lupu C, Lupu F. Extracellular protein disulfide isomerase regulates coagulation on endothelial cells through modulation of phosphatidylserine exposure. *Blood.* 2010;116(6):993-1001.
32. Edgell CJ, McDonald CC, Graham JB. Permanent cell line expressing human factor VIII-related antigen established by hybridization. *Proc Natl Acad Sci U S A.* 1983;80(12):3734-3737.
33. van Oost BA, Edgell CJ, Hay CW, MacGillivray RT. Isolation of a human von Willebrand factor cDNA from the hybrid endothelial cell line EA.hy926. *Biochem Cell Biol.* 1986;64(7):699-705.
34. Ling S, Dai A, Williams MR, et al. Testosterone (T) enhances apoptosis-related damage in human vascular endothelial cells. *Endocrinology.* 2002;143(3):1119-1125.
35. Silasi-Mansat R, Zhu H, Popescu NI, et al. Complement inhibition decreases the procoagulant response and confers organ protection in a baboon model of Escherichia coli sepsis. *Blood.* 2010;116(6):1002-1010.
36. Thyberg J. Caveolae and cholesterol distribution in vascular smooth muscle cells of different phenotypes. *J Histochem Cytochem.* 2002;50(2):185-195.
37. Westmuckett AD, Lupu C, Roquefeuil S, Krausz T, Kakkar VV, Lupu F. Fluid flow induces upregulation of synthesis and release of tissue factor pathway inhibitor in vitro. *Arterioscler Thromb Vasc Biol.* 2000;20(11):2474-2482.
38. Daum JR, Wren JD, Daniel JJ, et al. Ska3 is required for spindle checkpoint silencing and the maintenance of chromosome cohesion in mitosis. *Curr Biol.* 2009;19(17):1467-1472.
39. Seo J, Kim J, Kim M. Cloning of androgen-inducible gene 1 (AIG1) from human dermal papilla cells. *Mol Cells.* 2001;11(1):35-40.
40. Zhang X, Yu H, Lou JR, et al. MicroRNA-19 (miR-19) regulates tissue factor expression in breast cancer cells. *J Biol Chem.* 2010;286(2):1429-1435.
41. Wang Q, Li W, Liu XS, et al. A hierarchical network of transcription factors governs androgen receptor-dependent prostate cancer growth. *Mol Cell.* 2007;27(3):380-392.
42. Koochekpour S. Androgen receptor signaling and mutations in prostate cancer. *Asian J Androl.* 2010;12(5):639-657.
43. Aoki H, Seki T, Sawada J, Handa H, Adachi K. The promoter of an androgen dependent gene in the hamster flank organ. *J Dermatol Sci.* 1997;15(1):36-43.
44. Lu ML, Schneider MC, Zheng Y, Zhang X, Richie JP. Caveolin-1 interacts with androgen receptor. A positive modulator of androgen receptor mediated transactivation. *J Biol Chem.* 2001;276(16):13442-13451.
45. Cinar B, Mukhopadhyay NK, Meng G, Freeman MR. Phosphoinositide 3-kinase-independent non-genomic signals transit from the androgen receptor to Akt1 in membrane raft microdomains. *J Biol Chem.* 2007;282(40):29584-29593.
46. Loss ES, Jacobsen M, Costa ZS, Jacobus AP, Borelli F, Wassermann GF. Testosterone modulates K(+)ATP channels in Sertoli cell membrane via the PLC-PIP2 pathway. *Horm Metab Res.* 2004;36(8):519-525.